Surface-Wave Supervirtual Seismic Interferometry
the Ugly, the Bad, and the Good

Hassing, S.; Draganov, D.; Verschuur, E.

DOI
10.3997/2214-4609.202420118

Publication date
2024

Document Version
Final published version

Citation (APA)
Hassing, S., Draganov, D., & Verschuur, E. (2024). *Surface-Wave Supervirtual Seismic Interferometry: the Ugly, the Bad, and the Good* . Paper presented at Near Surface Geoscience 2024, Helsinki, Finland. https://doi.org/10.3997/2214-4609.202420118

Surface-wave supervirtual seismic interferometry: the ugly, the bad, and the good

S. Hassing[1], D. Draganov[1], E. Verschuur[1]

[1] TU Delft

Summary

We apply supervirtual interferometry to boost the surface-wave content of two different seismic surveys. The method uses seismic interferometric principles to exploit data redundancy in multi-fold surveys. The effect on the first survey is generally positive, where the signal-to-noise ratio is improved and the relative amplitude of other events, like direct waves or reflections, is decreased. The second survey shows that the effects are not always positive. For some shots, the quality of the dispersion curve decreases and for some a higher mode becomes more dominant. This can be caused when assumptions made for seismic interferometry by corrrelation are not complied with, primarily heterogeneities in the medium and attenuation. As such, the effect of applying supervirtual interferometry could be used as an indication for local heterogeneities.

Surface-wave supervirtual seismic interferometry: the ugly, the bad, and the good

As the majority of energy originating from a seismic source at the surface is transformed into surface waves, these also form a large part of the correlated noise for seismic reflection surveys. For surface-wave surveys, however, this is a major advantage. During such a survey, the dispersive properties of surface waves are exploited to get a measure of how the seismic-velocity structure of the subsurface changes with depth. For most geotechnical applications, this is done in a workflow called Multichannel Analysis of Surface Waves (MASW, Park et al., 1999).

For such an analysis, the data, recorded along a line with a source and several receivers, is transformed to the frequency-phase velocity domain (the dispersion spectrum), where maxima (the dispersion curve) indicate propagation of surface waves. These maxima are then used as input for a one-dimensional inversion to obtain a shear-wave velocity profile for this set of receivers (e.g., Xia et al., 1999; Wathelet et al., 2004). These profiles are then combined to obtain a multidimensional velocity structure.

Even though the surface waves may be the strongest event in the recording, surface-wave surveys still often suffer from problems with noise. It is possible the extend the receiver line used to create the dispersion spectrum, but this also leads to a loss of lateral resolution. Supervirtual interferometry (SVI) is an alternative method, based on seismic interferometry.

Originally, this method was applied to refraction surveys (Mallinson et al., 2011; Bharadwaj et al., 2012), but can also be applied for surface waves (Xu et al., 2017), in fact for every event recorded by the receivers that originates from the same stationary-phase region. We apply SVI to two datasets with the aim to boost the surface-wave content of the data and investigate how the process affects the resulting data.

Theory

The basic principle of seismic interferometry is that by crosscorrelating two traces, sharing the travelpath of the same event, the Green's function would be retrieved that results if the (virtual) source were located at the first receiver location and its response recorded at the second location (Wapenaar and Fokkema, 2006). Furthermore, when using transient sources, these sources should be placed on a surface with smooth velocity variations surrounding the receivers and the medium of interest and then summed to obtain the full Green's function.

For surface waves, when we assume only smooth and relatively small lateral variations in the velocity structure of the medium under consideration (as we also do to apply MASW), all receivers can be placed on a line and the sources on the line on both sides of the receiver.

SVI uses this concept to exploit the data redundancy of using multiple shots. The process consists of two steps, as illustrated in Figure 1. During the first step, the same two receivers are crosscorrelated and summed for every source position on one side of the receivers. This gives a trace where all constructive events propagating between the two receivers are boosted.

During the second step, the original trace recorded at the second receiver position is recreated by 'attaching' two traces together using seismic interferometry by convolution. The first trace is the one recorded at the first receiver and resulting from the original source position. The second is the trace resulting from the virtual source located at the first receiver position and recorded at the second. This can be repeated for every virtual-source position between the original source position and the second receiver and summed. This gives a second increase in signal-to-noise ratio.

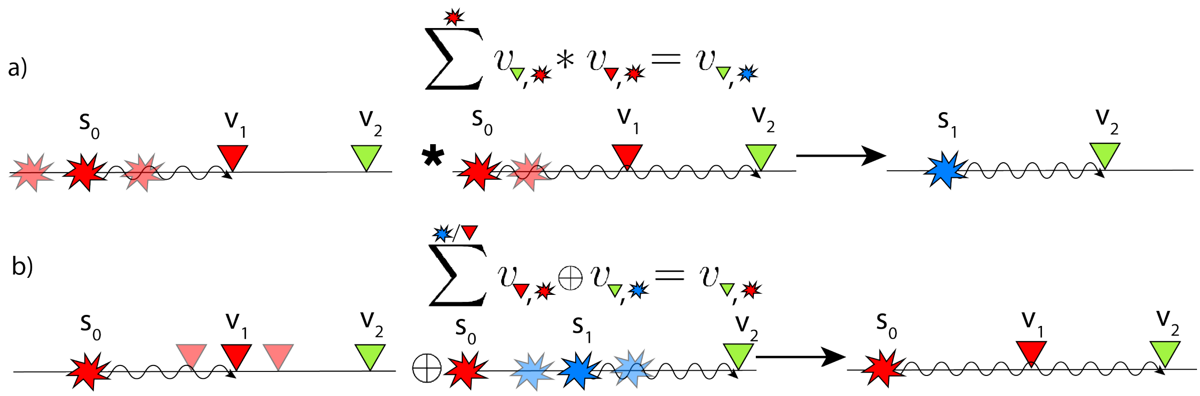

Figure 1: The basic concept of supervirtual interferometry. **a)** shows the first step where receiver v_1 is crosscorrelated ($*$) with receiver v_2 for each shot position to the left of v_1. This results in virtual shot position s_1 recorded at v_2 and is summed to boost the signal-to-noise ratio. **b)** shows the second step, where it is possible to convolve ($\oplus$) the trace recorded at receiver v_1 from real source s_0 with the trace recorded at receiver v_2 from virtual source s_1 at the same position as r_1 to reobtain the trace recorded at receiver v_2 originating from source s_0. This can be repeated for every possible receiver position between the source s_0 and receiver v_2 and summed to increase the signal-to-noise ratio a second time.

Methods

We apply SVI to two different datasets. The first is a small part of the SCAN project from the centre of the Netherlands (Rehling et al., 2023). Specific characteristics of the data can be found in Table 1. To decrease the amount of data to work with, the full dataset has been subsampled to a rate of 100 Hz and a lowpass filter at 20 Hz has been applied. The signal-to-noise ratio is relatively high and the surface wave can clearly be distinguished. A downside is that not all source locations could be on the receiver line. A minimum offset of 500 m is used as the off-line effects are less noticeable. After 2000 m offset, the main surface-wave arrival is no longer included in the data, so this offset is used as a maximum.

The second dataset, simply called the Farm data here, is from a shorter, but more densely sampled receiver line. The signal-to-noise ratio is lower, the surface waves are less consistent, and the direct P-wave is stronger. Offsets from 12 to 250 m are used for this dataset. A minimum offset is still enforced to remove near-field effects.

During the first step of SVI, instead of using crosscorrelation, we use crosscoherence, as this has shown to lead to an increased resolution for refraction imaging (Place et al., 2019). Where crosscorrelation is an element-wise multiplication in the frequency domain, for crosscoherence the frequency spectrum is first normalised by dividing by its absolute value. To compute the dispersion spectrum for the data, the Frequency-Domain Beamforming method is used (Zywicki and Rix, 2005).

Table 1: Survey characteristics for the two datasets

	SCAN data	Farm data
Receiver spacing [m]	5	3
Number of receivers	1500	507
Total line length [m]	7500	1521
Source spacing [m]	∼50	3
Number of shots	302	517
Sampling frequency [Hz]	100	500
Length of record [s]	7	5

Results

An example of a shot from the SCAN data before and after application of SVI is shown in Figure 2. The amplitude of both random noise and other events relative to the amplitude of the surface waves has decreased after SVI. The direct wave and the reflections that are visible in Figure 2a are no longer visible in Figure 2b. Similarly, the secondary event visible at 2000m offset and 6 s two-way traveltime is averaged out by SVI and no longer visible in Figure 2b. The dispersion spectrum has also visibly improved in quality. It is more continuous and shows less random noise.

Roughly similar effects can be observed for the Farm data in Figure 3. Generally, the surface waves are boosted and random noise damped. However, the dispersion spectrum shows that the effects are more complex. Some shots show clear improvement, some show a changed dispersion curve, while others even show a degradation in the dispersion curve.

An example of the changed dispersion curve is shown in Figure 3 along with the shots. The fundamental mode of the dispersion curve extends to roughly 23 Hz in the original shot, but only to 16 Hz in the SVI-adapted shot. On the other hand, the higher mode that is also visible in the original shot above this frequency limit also extends to the new frequency limit. The fundamental mode can still be observed at 20 Hz, but is overshadowed by the stronger higher mode.

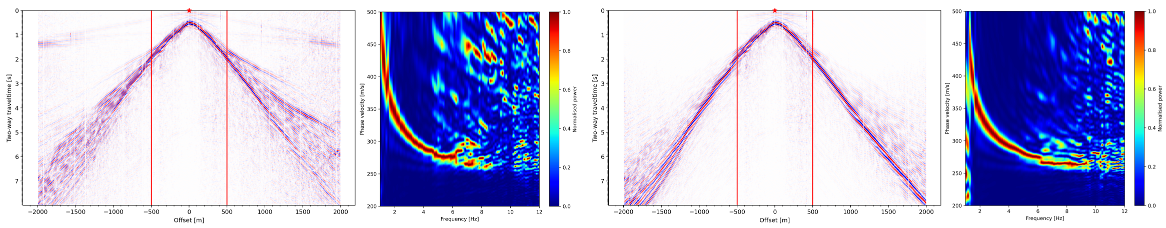

(a) (b)

Figure 2: A shot from the SCAN section at around 3000 m along the line **(a)** before and **(b)** after the application of SVI with its corresponding dispersion spectrum. Note that the offsets between the red lines were not included in the SVI process or in the calculation of the dispersion spectrum, but are included for plotting purposes. A comparison shows that the relative amplitude of both the random noise and of other events like the direct wave and reflections has diminished and the dispersion curve is more consistent and less noisy.

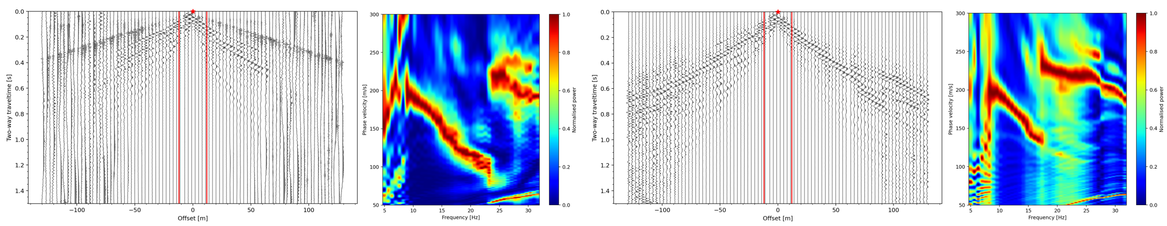

(a) (b)

Figure 3: A shot from the Farm data at around 190 m along the line **(a)** before and **(b)** after application of SVI with its corresponding dispersion spectra. Offsets between the red lines were not included in the SVI process. A comparison shows that for example the low-frequency noise is diminished and the strong event travelling at 340 m/s (presumably the air wave) has disappeared. The fundamental mode can be observed only to a lower frequency after SVI, while a higher mode appears to be dominant in this range.

Discussion

Generally, SVI offers an improvement on the original data, but not in every case. This is mainly caused by non-compliance with assumptions used for seismic interferometry. One of these assumptions is that the sources should be placed on a surface with smoothly varying velocity surrounding the receivers and medium of interest. In reality, the sources are placed along the line of receivers. Sudden variations in medium properties along the source locations will distort the results of SVI.

A second assumption not complied with is that in reality attenuation of the propagating wave can play a significant role. With increasing distance, higher frequencies are damped more than lower ones, while for seismic interferometry by crosscorrelation (and thus crosscoherence), these effects are not taken into account. This means that sources further away from the target area will contribute to the lower-frequency events, but less if at all to the high-frequency events. This could also be related to the observation that the higher mode becomes dominant over the fundamental mode at more frequencies after application of SVI. Another implication is that the changes observed after application of SVI can serve as an indicator for heterogeneity in the medium.

Conclusions

In order to boost the surface-wave content of seismic data, we applied supervirtual interferometry, a method that exploits data redundancy in multi-fold surveys with seismic interferometry to enhance the signal-to-noise ratio. We applied the method to two different surveys. The first survey shows generally positive effects. The second survey, however, shows that the effects are not always positive. This is mostly related to where assumptions made for seismic interferometry are not valid in the field and could be used to indicate heterogenities in the medium.

Acknowledgements

We gratefully acknowledge EBN for providing the SCAN data and Near Surface Investigations, LLC, for providing the Farm data used in this work. We also thank the sponsors of the Delphi consortium for their support.

References

Bharadwaj, P., Schuster, G., Mallinson, I. and Dai, W. [2012] Theory of Supervirtual Refraction Interferometry: Theory of SVI. *Geophysical Journal International*, **188**(1), 263–273.

Mallinson, I., Bharadwaj, P., Schuster, G. and Jakubowicz, H. [2011] Enhanced Refractor Imaging by Supervirtual Interferometry. *The Leading Edge*, **30**(5), 546–550.

Park, C.B., Miller, R.D. and Xia, J. [1999] Multichannel Analysis of Surface Waves. *GEOPHYSICS*, **64**(3), 800–808.

Place, J., Draganov, D., Malehmir, A., Juhlin, C. and Wijns, C. [2019] Crosscoherence-Based Interferometry for the Retrieval of First Arrivals and Subsequent Tomographic Imaging of Differential Weathering. *GEOPHYSICS*, **84**(4), Q37–Q48.

Rehling, J., Zaalberg-Metselaar, G., Peenstra, R., Van Den Akker, J. and Ter Borgh, M. [2023] The Dutch SCAN Geothermal Exploration Programme — The First Three Years of 2D Seismic Acquisition and (Re)Processing. *First Break*, **41**(1), 33–43.

Wapenaar, K. and Fokkema, J. [2006] Green's Function Representations for Seismic Interferometry. *GEOPHYSICS*, **71**(4), SI33–SI46.

Wathelet, M., Jongmans, D. and Ohrnberger, M. [2004] Surface-wave Inversion Using a Direct Search Algorithm and Its Application to Ambient Vibration Measurements. *Near Surface Geophysics*, **2**(4), 211–221.

Xia, J., Miller, R.D. and Park, C.B. [1999] Estimation of Near-surface Shear-wave Velocity by Inversion of Rayleigh Waves. *GEOPHYSICS*, **64**(3), 691–700.

Xu, Z., Juhlin, C., Han, L. and Zhang, F. [2017] Reconstruction of Surface Waves Using Super Virtual Interferometry: An Example from the Forsmark Site, Sweden. *Geophysical Journal International*, **211**(1), 120–140.

Zywicki, D.J. and Rix, G.J. [2005] Mitigation of Near-Field Effects for Seismic Surface Wave Velocity Estimation with Cylindrical Beamformers. *Journal of Geotechnical and Geoenvironmental Engineering*, **131**(8), 970–977.